Int J Adv Manuf Technol (2015) 76:229–246
DOI 10.1007/s00170-014-5887-3

ORIGINAL ARTICLE

Dynamic design methodology of high speed micro-spindles for micro/meso-scale machine tools

Guanghui Zhang · Kornel F. Ehmann

Received: 1 January 2014 / Accepted: 17 April 2014 / Published online: 10 May 2014
© Springer-Verlag London 2014

Abstract With the increasing demands for high manufacturing accuracy and processing efficiency, micro/meso-scale machine tool systems are proposed. The availability of micro-spindles with ultra-high rotating angular speeds and ultra-small run-out are a key technology for micro/meso-scale cutting processes. Well-established design methods exist for traditional spindle systems, but there is a strong demand for a methodology to predict the dynamic characteristics, particularly at the micro-scale, which will dictate manufacturing accuracy. In this respect, the minimization of run-out is of paramount importance. In response to this, two problem areas are considered in this paper: (a) hybrid air bearing systems—a methodology related to the calculation of the load capacity and stiffness of hybrid air journal and thrust bearings, and (b) spindle rotor system—a methodology for the rotor dynamic analysis including critical speed, mode shape, and unbalanced response predictions. Mathematical models and simulation procedures are given, followed by explanations of their use. Finally, the proposed dynamic design method is demonstrated on a realized micro-spindle system model. Two designs namely the original design and a modified design are analyzed and comparisons are carried out. The numerical simulations and the experimental evidence available for the original design have substantiated the validity of the proposed dynamic design method. The proposed methodology lays the foundation for controlling run-out of the high speed micro-spindles in micro/meso-scale machine tools.

G. Zhang (✉)
School of Energy Science and Engineering, Harbin Institute of Technology, Harbin, China
e-mail: zhanggh@hit.edu.cn

K. F. Ehmann
Department of Mechanical Engineering, Northwestern University, Evanston, IL, USA

Keyword Dynamic · Micro spindle · Micro air bearing · Rotor dynamic · Run-out

Nomenclature

e	Eccentricity for journal bearing
h	Air film thickness
h_{in}	The initial mounting clearance for thrust bearing
h_m	Average air film thickness
$\overline{h}$	Dimensionless air film thickness
k	The ratio of specific heat
l	The length of the journal bearing
$\dot{m}_i$	The mass flow through the ith orifice
p	Air film pressure
p_a	Atmospheric pressure
p_r	Reference air pressure
p_s	Supply pressure
r	The radius coordinate in cylindrical coordinate
$\overline{r}$	The dimensionless radius coordinate in cylindrical coordinate
t	Time
$\overline{t}$	Dimensionless time
$u.v,w$	Velocity of the air flow in x,y,z direction
$\overline{v}$	The velocity of air through the orifice
x, y, z	Cartesian coordinates
$\overline{x}, \overline{y}, \overline{z}$	Dimensionless Cartesian coordinates
$A_{orifice}$	The cross section area for the orifices
K_b	The stiffness for the bearing
$\overline{Q}$	The flow factor for orifices
R_1	The inner radius for thrust bearing
R_2	The outer radius for thrust bearing
W	The load capacity for the bearing
β_i	The pressure ratio
δ_i	Kronecker symbol
ε	The eccentricity ratio for journal bearing
η	The dynamic viscosity of lubricated air

θ	The angular coordinate
$\theta_X\,\theta_Y$	The tilting angle for thrust plate along X and Y direction
ρ	The air density under arbitrary pressure
ρ_a	The air density under atmospheric pressure
σ	Bearing number for transient analysis
φ	The attitude angle
ψ	Flow coefficient of the orifice
Λ	The bearing number for thrust bearing
Λ_x	The bearing number in x direction
Λ_z	The bearing number in z direction
Φ	The discharge coefficient
Ω	Rotating angular speed

1 Introduction

As the applications of miniature components with 3D features in industries ranging from aerospace to biomedical that are made from a wide range of engineering materials including steel, titanium, aluminum and brass, to mention a few, the demand for high precision and high performance manufacturing machines increases. In response to these needs, micro/meso-scale machine tools (mMT for short) were proposed to decrease the machine size, increase the accuracy and reduce the cost [1]. For micro material cutting processes, the micro-spindle is the most critical component that provides the rotating tool motion with rotating angular speeds approaching 10^6 rpm. For micro-spindles, another significant performance index is their run-out. An example of a designed and manufactured micro-spindle that reached a maximal speed of approximately 420,000 rpm is given in [2]. The main challenge reported remained the reduction of run-out. To further enhance micro-spindle performance, it is necessary to have a well-defined systematic design methodology. Such a design methodology, to meet the desired dynamic characteristics of the micro-spindles in mMT applications, will be proposed in this paper.

The FANUC Corporation [3] designed and manufactured an air turbine spindle for the ROBOnano (Super Nano Machine) whose rotational speed reached 70,000 rpm in which aerostatic bearings were employed. If higher rotating speeds could be obtained, productivity and accuracy could be significantly improved. The Atometric Company [4] developed a micro machining center with a micro-spindle with a maximal speed of 200,000 rpm, while Microlution [5] developed a micro-spindle driven by an electrical motor which could reach 40,000 rpm. A rotating speed of 160,000 rpm was available if an air turbine was used. For the high speed micro-spindles, hydrostatic air bearings were employed.

The above examples suggest that significant benefits could be accrued from the development of high speed micro-spindles. This, in turn, as stated above, necessitates suitable design techniques and methodologies. Because of their particular physical properties, spindles using air bearings could offer high rotating speeds, low friction and durable operation. Also, they have the potential to yield design solutions that result in low run-out, which is a significant prerequisite for achieving high accuracy. In the paragraphs that follow, a brief review of the literature related to these two key topics issues be presented.

Zhang et al. [6] investigated the effect of spindle vibrations on surface quality in raster milling, where aerostatic bearings were employed and the impulsive excitation by the cutting force was considered. Their numerical and experimental study has indicated that the vibrations would produce complex patterns like run-out on a surface. The work laid the foundation for optimization leading to the appropriate selection of the spindle speed. In the study, the spindle rotor was assumed as a lumped mass model without considering the elastic deformations of the rotor. Martin et al. [7] and Marsh [8], in turn, investigated the impact of spindle vibrations on surface topography. A five-degrees-of-freedom dynamic model for an aerostatic bearing spindle for studying the vibrations of the spindle system was proposed by Zhang et al. [9]. The effect of the vibrations on surface topography in ultra-precision diamond turning was discussed. They have found that the motion of the spindle had a different effect on surface topography for different cutting processes. An et al. [10] studied the stability of the axis orientation of aerostatic spindles in fly cutting machines. In their study, the tilting motion of the spindle was not included. The theoretical analysis results have been verified by experiments on an actual machine.

To assess the performance of air bearings, Bhat et al. [11] investigated inlet restrictor design methods to satisfy the demands of precision and ultra-precision manufacturing. The static and dynamic characteristics of the aerostatics bearing were obtained. To overcome the shortages of the traditional perturbation methods of nonlinear analysis, Hassini et al. [12] proposed a method based on a frequency-dependent analysis. The results indicated that the proposed method was in good agreement with the solution of the full nonlinear Reynolds equation. A type of aerostatic bearing with compound restrictors for manufacturing small holes on printed circuit boards was proposed by Otsu et al. [13]. These restrictors had greater stiffness than the traditional inherent restrictors. It was shown that aerostatic bearings with compound restrictors had a much higher threshold speed. Liu et al. [14] employed Newton's method for linearizing the Reynolds equation to study the performance of externally pressurized air bearings for spindles. The pressure distribution, load capacity, and stiffness were obtained. The coupling between the aerostatic and aerodynamic effects was also investigated. It was indicated that rotational effects could not be ignored when the spindle speed is high. To obtain the static and dynamic characteristics

of the hybrid journal gas bearing simply, quickl,y and accurately, Zhang et al. [15] proposed an analytical force parameters identification method. By employing the Laplace transform, the stiffness and damping could be obtained.

For the dynamic characteristics of the air bearing rotor system, Chen et al. [16] studied the performance of a rigid spindle rotor aerostatic bearing system, where orifices and inherent compensations were employed. The static equilibrium position and stability of the system were obtained, and the effect of the arrangement of the air entries on bearing characteristics was analyzed. It was shown that an optimum design of the aerostatic bearing could be acquired. Delhaes et al. [17] proposed a new type of air turbine spindle called the viscous driven aerostatic supported spindle for micro milling operations. The optimization for the system design and its preliminary experimental verification was carried out. A maximal rotating speed of 24,000 rpm was obtained. Wang [18] employed a numerical method to investigate the bifurcation characteristics of the spindle air bearing system. The results indicated that complex nonlinear behaviors such as sub-harmonic and quasi-periodic motions could be observed for the operation of the spindle system. A hybrid numerical method to study the nonlinear characteristics of high speed spindle air bearing systems was proposed by Wang et al. [19]. It was shown that the proposed method could be an effective way to predict the dynamic performance of the system. Al-bender [20] modeled and analyzed the dynamic characteristics of aerostatic bearing films, based on which an active dynamic compensation method was proposed to improve the stability of the system. The results proved that the study provides a basis for designing and implementing an active control method. Yang et al. [21] studied the influence of the orifices' parameters (including their number and location) on the stability of the aerostatic bearing-rotor system, assuming a rigid rotor. Different optimization procedures were carried out for achieving a maximal stability threshold and maximal load capacity. Zhang proposed the forecasting orbit method to obtain the nonlinear characteristics of the air bearing-rotor system for a self-acting gas bearing [22] and a hybrid gas bearing [23]. It was indicated that complex behaviors such as whirling instability could be observed by employing the proposed method, which laid the foundation for understanding of the air bearing spindle system. But the forecasting orbit method is time consuming limiting, thereby, its applications. Schiffmann et al. [24] studied an integrated design and optimization method for gas bearing rotor systems, in which the interaction between the rotor and the gas bearing was considered. By employing the proposed method, the characteristics of the system were significantly improved, especially its stability margin.

To control run-out in spindles used in mMTs, a dynamic design methodology for air bearing spindle systems is proposed and studied in this paper. A design methodology for micro hybrid bearing integrated with Newton's linearization method and the finite difference method is presented to reduce simulation time and increase accuracy. A modeling and solution technique for the micro spindle rotor system that considers its elastic deformations is also established. Elastic deformations are usually ignored in traditional spindle dynamics analysis. The transfer of variables between the bearing design and the spindle rotor dynamic design is clarified to yield a seamless design approach for micro spindle systems. To illustrate the validity of the proposed methodologies, the improvements of an existed design will be carried out and a comparison between the existing and the modified design will be presented.

The remainder of the paper is divided into several sections. The basic configuration of the spindle system is highlighted in Section 2. In Section 3, the design methodologies for the air bearings, i.e., the journal bearing and thrust bearing are presented. Newton's method is employed for the linearization of the generalized Reynolds equation for the flow in the clearances. The load capacity, static equilibrium position, and stiffness coefficients are acquired. The subsequent section, Section 4, presents the modeling methodology for the rotor dynamics of the spindle system. The elastic deformations and gyroscopic effects of the spindle are also included. The model for the spindle rotor is established by the finite element method. The critical speeds, mode shapes and dynamic responses are evaluated. The original and modified designs of the spindle system are analyzed by the proposed methodologies. Section 5 summarizes the proposed integrated design methodology, while Section 6 draws some brief conclusions.

2 Basic configuration of a high speed micro-spindle system

The basic structure/configuration of a high speed micro-spindle is presented in Fig. 1, which is quoted from Ref. [2]. The dynamic design methodologies that will be presented in this paper will use this model to prove the validity of the proposed methods. From the viewpoint of dynamic design, the two journal/thrust bearings and the shaft/turbine/thrust pad to be referred to as the one piece rotor constitute the principal components of the system. Bearing no. 1 is located at the tool clamping end, while bearing no. 2 is at the free end of the spindle. The O-rings are employed for sealing and adding damping to the system. As reported in Ref. [2], a developed prototype micro-spindle of this configuration reached a maximal speed of about 420,000 rpm. But, the run-out of about 3 μm at the maximal speed remained as a major challenge for the spindle.

To overcome the performance limitations of this design, a dynamic design methodology for micro-spindle systems will be presented that addresses the following issues: (a) the dynamic characteristics of the thrust and journal bearings, and (b) modeling and simulation of the motion of the spindle rotor. Subsequently, a comparison between the original design and a

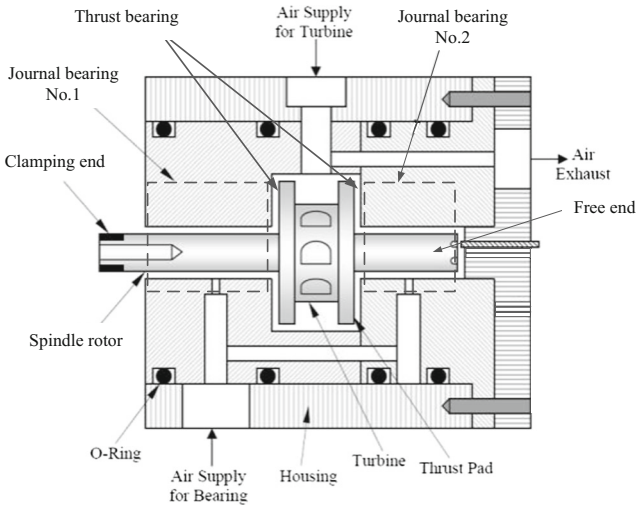

Fig. 1 Basic structure of the high speed micro-spindle

modified design based on the proposed methods will be presented.

3 Dynamic design of micro hybrid air bearings

3.1 Mathematical modeling of the flow in the clearances

As mentioned in Ref. [2], for micro air bearings of the spindle for mMTs, the modified Reynolds number is approximately 0.1 and the Knudsen number is on the order of 0.001. Consequently, the classical fluid equations that neglect inertia effects and hold the continuum hypothesis can be employed. It should also be noted that the mathematical modeling of micro air bearings is more complex than that of the liquid film bearings owing to the compressibility of air. Therefore, the assumptions to be employed in this paper are the following:

(a) the variation of viscosity and density in the film thickness direction is ignored
(b) the flow is isothermal
(c) the inertia and body forces are neglected

3.1.1 Governing equation and its dimensionless form for micro journal bearings

The classical Reynolds equation for micro hybrid air journal bearings in Cartesian coordinates is given by [14]:

$$\frac{\partial}{\partial x}\left(h^3 p\frac{\partial p}{\partial x}\right)+\frac{\partial}{\partial z}\left(h^3 p\frac{\partial p}{\partial z}\right)+12\delta_i\eta\rho\frac{p_a}{\rho_a}\,\bar{v} = 12\eta\frac{\partial(ph)}{\partial t}+6\eta u\frac{\partial(ph)}{\partial x}+6\eta w\frac{\partial(ph)}{\partial z} \tag{1}$$

with the film thickness expression:

$$h = h_m(1+\varepsilon\cos(\theta-\varphi)) \tag{2}$$

where δ_i denotes the location of the orifices. It equals to 1 at the location of the orifice and 0 at positions without orifices.

The air through the orifices is assumed as a point source with a mass flow rate of:

$$\dot{m}_i = \Phi p_s A_{orifice}\sqrt{\frac{2\rho_a}{p_a}}\psi \tag{3}$$

$$\psi = \begin{cases} \left[\frac{k}{k-1}\left(\beta_i^{2/k}-\beta_i^{(k+1)/k}\right)\right]^{1/2} & \beta_i > \beta_k \\ \frac{k}{2}\left(\frac{2}{k+1}\right)^{(k+1)/k-1} & \beta_i \le \beta_k \end{cases} \tag{4}$$

where $\beta_k = \left(\frac{2}{k+1}\right)^{k/k-1}$

By introducing dimensionless parameters in Cartesian coordinates:

$$\overline{p} = p/p_r, \overline{h} = h/h_m, \overline{x} = x/l, \overline{z} = z/l, \overline{t} = t\overline{v}/l$$

the following dimensionless variables can be defined:

$$\Lambda_x = \frac{12\eta u l}{h_m^2 p_r}, \Lambda_z = \frac{12\eta w l}{h_m^2 p_r}, \sigma = \frac{24\eta\overline{v}l}{h_m^2 p_r}, \overline{Q} = \frac{24\eta l^2 p_a\rho\overline{v}}{h_m^3 p_r^2\rho_a}$$

which yield the dimensionless Reynolds equation for micro journal bearings in the form:

$$\frac{\partial}{\partial\overline{x}}\left(\overline{h}^3\frac{\partial\overline{p}^2}{\partial\overline{x}}\right)+\frac{\partial}{\partial\overline{z}}\left(\overline{h}^3\frac{\partial\overline{p}^2}{\partial\overline{z}}\right)+\overline{Q}\delta_i = \Lambda_x\frac{\partial(\overline{p}\overline{h})}{\partial\overline{x}} + \Lambda_z\frac{\partial(\overline{p}\overline{h})}{\partial\overline{z}}+\sigma\frac{\partial(\overline{p}\overline{h})}{\partial\overline{t}} \tag{5}$$

By ignoring the transient term and the flow along the axial direction, the Reynolds equation for micro journal bearings can be simplified and written in its final form as:

$$\frac{\partial}{\partial\overline{x}}\left(\overline{h}^3\frac{\partial\overline{p}^2}{\partial\overline{x}}\right)+\frac{\partial}{\partial\overline{z}}\left(\overline{\overline{x}}^3\frac{\partial\overline{p}^2}{\partial\overline{z}}\right)+\overline{Q}\delta_i = \Lambda_x\frac{\partial(\overline{p}\overline{x})}{\partial\overline{x}} \tag{6}$$

3.1.2 Governing equation and its dimensionless form for micro thrust bearings

For the micro thrust bearings, cylindrical coordinates are applied. The Classical Reynolds equation for micro thrust bearings is as follows [25]:

$$\frac{1}{r}\frac{\partial}{\partial r}\left(rh^3p\frac{\partial p}{\partial r}\right)+\frac{1}{r^2}\frac{\partial}{\partial\theta}\left(h^3p\frac{\partial p}{\partial\theta}\right)+12\eta\delta_i\frac{p_a}{\rho_a}\rho\tilde{v}=6\eta\omega\frac{\partial(ph)}{\partial\theta} \quad (7)$$

where δ_i, as before, denotes the location of the orifices and is again equal to 1 at the orifice location and equal to 0 elsewhere. The mass flow rate through the orifices is presented by Eq. (3) and Eq. (4).

By introducing the dimensionless parameters in cylindrical coordinates:

$$\overline{h}=\frac{h}{h_m},\overline{r}=\frac{r}{R_2},\overline{p}=\frac{p}{p_r}$$

the following dimensionless variables can be defined:

$$\Lambda=\frac{6\eta\omega}{p_r}\left(\frac{R_2^2}{h_m^2}\right),\overline{Q}=\frac{12\eta R_2^2p_a}{\rho_a h_m^3p_r^2}\rho\overline{v}$$

leading to the dimensionless Reynolds equation for micro thrust bearings:

$$\frac{1}{\overline{r}}\frac{\partial}{\partial\overline{r}}\left(\overline{r}\overline{h}^3\overline{p}\frac{\partial\overline{p}}{\partial\overline{r}}\right)+\frac{1}{\overline{r}^2}\frac{\partial}{\partial\theta}\left(\overline{h}^3\overline{p}\frac{\partial\overline{p}}{\partial\theta}\right)+\overline{Q}\delta_i=\Lambda\frac{\partial(\overline{p}\overline{h})}{\partial\theta} \quad (8)$$

In a manner similar to the case of micro journal bearings, a film thickness expression is also required for the micro thrust bearings. To define such an expression, the tilt of the thrust disk of the rotor needs to be considered. The tilt of the rotor can be defined by the angle around the x axis, θ_X, and the angle around the y axis, θ_Y, as shown in Fig. 2.

Since the angles θ_X and θ_Y are relatively small, it can be assumed that $\theta_X\approx\sin\theta_X,\theta_Y\approx\sin\theta_Y$ so that the film thickness as a function of the tilting state of the rotor can be expressed as follows:

$$h=h_{in}+\theta_X r\sin\varphi-\theta_Y r\cos\varphi \quad (9)$$

where h_{in} is the initial mounting clearance of the thrust bearing.

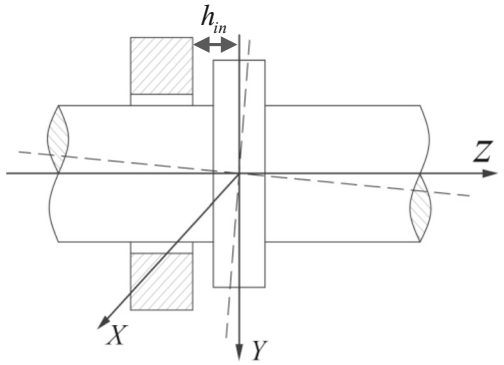

Fig. 2 Tilting of the thrust disk for thrust bearings

3.1.3 Newton's method of linearization

The dimensionless Reynolds equations for the micro journal and thrust bearings, presented in Sections 3.1.1 and 3.1.2, are nonlinear equations. Consequently, Newton's method and the associated iterative process will be employed to solve Eq. (6) and Eq. (8). Newton's method has the advantage of decreasing simulation time and leading to fast convergence when the film thickness is small, which is a typical characteristic of micro bearings. For the micro bearings of the micro-spindle system, the eccentricity ratio is usually small and the rotating speed is high (e.g., in excess of 400,000 rev/min as indicated above). For high rotating speeds of the micro hybrid journal and thrust air bearings, initial data/conditions are required to accelerate convergence. To meet this requirement, the simulations are started at a small rotating speed, and the pressure distribution is obtained. Then, the simulation moves to increasingly higher rotating speeds, where the pressure distribution computed at the lower rotating speed is used as the initial value.

The detailed configuration of an externally pressurized air bearing is shown in Fig. 3. Figure 3a shows the cross-section of the journal bearing. In the current work, six orifices arranged in the circumferential direction at 60° intervals will be assumed. Figure 3b, in turn, depicts the cross section of the thrust bearing. Again, six orifices, arranged in the circumferential direction, are assumed. The arrangement of the orifices along the axial direction for the journal bearing is not presented. In the design procedure to be developed below, the number of orifices along the axial direction will be assumed as a variable that is changeable for optimization purposes.

The nonlinear function $F(\overline{p})$ in the Reynolds equation is defined as follows [14]:

(a) For journal bearings:

$$F(\overline{p})=\frac{\partial}{\partial\overline{x}}\left(\overline{h}^3\frac{\partial\overline{p}^2}{\partial\overline{x}}\right)+\frac{\partial}{\partial\overline{z}}\left(\overline{h}^3\frac{\partial\overline{p}^2}{\partial\overline{z}}\right)+\overline{Q}\delta_i-\Lambda_x\frac{\partial(\overline{p}\overline{h})}{\partial\overline{x}} \quad (10)$$

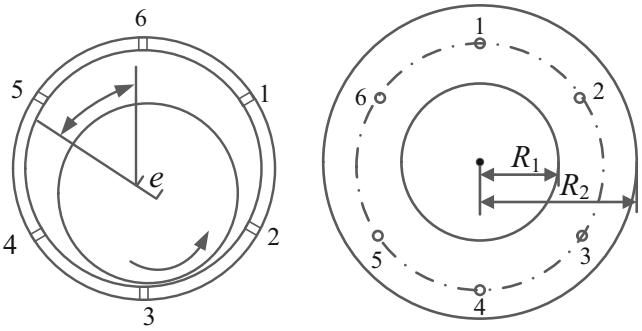

(a) Journal bearing (b) Thrust bearing

Fig. 3 Cross-section of micro externally pressurized air bearings

(b) For thrust bearings:

$$F(\bar{p}) = \frac{1}{\bar{r}}\frac{\partial}{\partial \bar{r}}\left(\bar{r}\bar{h}^3\bar{p}\frac{\partial \bar{p}}{\partial \bar{r}}\right) + \frac{1}{\bar{r}^2}\frac{\partial}{\partial \theta}\left(\bar{h}^3\bar{p}\frac{\partial \bar{p}}{\partial \theta}\right) + \bar{Q}\delta_i - \Lambda\frac{\partial(\bar{p}\bar{h})}{\partial \theta} \quad (11)$$

By applying Newton's iterative procedure, one obtains:

$$F(\bar{p}^n) + F'(\bar{p}^n)\left(\bar{p}^{n+1} - \bar{p}^n\right) = 0 \quad (12)$$

$$F'(\bar{p}^n)\delta^n = -F(\bar{p}^n) \quad (13)$$

where $\delta^n = \bar{p}^{n+1} - \bar{p}^n$

By employing the Taylor expansion:

$$F(\bar{p} + \beta\delta) = F(\bar{p}) + \beta\delta F'(\bar{p}) \quad (14)$$

Then,

$$\frac{dF(\bar{p} + \beta\delta)}{d\beta} = \delta F'(\bar{p}) = -F(p) \quad (15)$$

By substituting Eq. (14) into Eq. (10) and Eq. (11), the Reynolds equations for the journal and thrust bearings have been converted by Newton's method. Second order accurate finite difference formulas are employed to discretize the partial differential equation from Eq. (15). The successive relaxation method is used to update the pressure difference δ, defined by Eq. (13). More details about the procedure are included in Ref. [14].

The stiffness of the bearing is defined as the force per unit displacement or per unit rotation. The force can be obtained by integrating the pressure in the bearing, which is defined as ***W***.

The stiffness against displacement (such as the axial stiffness for thrust and radial stiffness for journal bearings) is defined as:

$$K_b = \frac{W(x + \Delta x) - W(x)}{\Delta x} = \frac{\Delta W}{\Delta x} \quad (16)$$

where x denotes the displacement of the shaft corresponding to the applied force.

The rotational stiffness for (e.g., the bending stiffness of thrust bearings) is defined as:

$$K_b = \frac{W(\chi + \Delta\chi) - W(\chi)}{\Delta\chi} = \frac{\Delta W}{\Delta\chi} \quad (17)$$

where χ denotes the rotation angle of the shaft corresponding to the applied force.

The flow chart of the calculations to obtain the pressure distributions for the journal and thrust bearings and their stiffness is shown in Fig. 4.

3.2 Micro thrust bearings—numerical simulation and discussion

By employing the proposed method in Section 3.1, the characteristics of micro thrust bearings can be obtained. The convergence residual is smaller than 10^{-6}. The detailed parameters for the micro thrust bearing are presented in Table 1 that correspond to the design presented in Ref. [2].

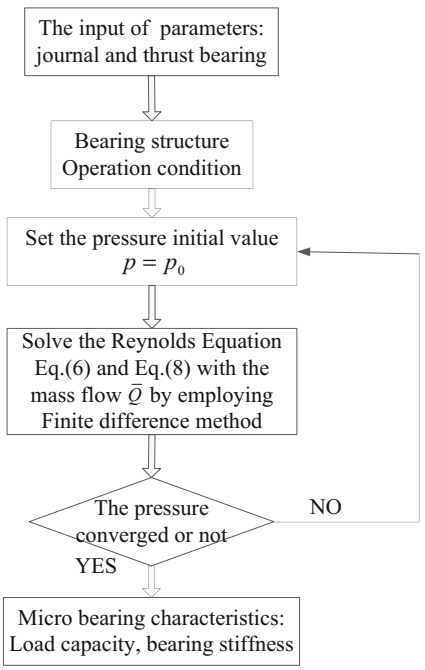

Fig. 4 The flow chart for the analysis of micro journal and thrust bearing

Table 1 Fundamental parameters for the micro thrust bearing

Variation name	Value
Outer diameter of the thrust bearing	15 mm
Inner diameter of the thrust bearing	7 mm
Rotating angular speed	600,000 rev/min
Absolute viscosity of air	1.73×10^{-5} N•s/m^2
Radius clearance for the thrust bearing	4 μm
Clearance for the two pads	8 μm
Diameter for the thrust bearing orifice	0.075 mm
Supply pressure	1.11 MPa
Radius for the circle of the orifices	5.5 mm
Number of orifices	6

The pressure distribution for the micro thrust bearing with the thrust plate located in the middle of the bearing is presented in Fig. 5. If the thrust plate is located in the middle of the bearing clearance, the pressure on the two thrust pads is the same and no thrust load force is generated. The pressure distribution in Fig. 5 depicts the pressure distribution on one pad. The pressure peaks that exist at the locations of the orifices will influence the load capacity of the bearing. Since the clearance of the bearing is small (about 4 μm), the pressure at the orifice is relatively high as compared to other regions of the clearance and it is nearly equal to the supply pressure. This means that the load capacity of the micro thrust bearing is mainly generated by the restriction of the orifices.

If the clearances of the two pads of the micro thrust bearing are different, the pressure distributions on the two pads will also be different. In other words, an axial displacement will result in a thrust force direction and manifest itself in the form of the axial stiffness. The thrust force will balance the axial force generated by the cutting process performed by the micro-spindle. In light of this, it is important to obtain the load capacity and axial stiffness in support of the dynamic design of the micro thrust bearings. By employing Eq. (16), the axial stiffness of the micro bearing can be obtained. In Fig. 6, the variation of the load capacity and axial stiffness as a function of the axial displacement is presented. As the axial displacement increases, the load capacity and the axial stiffness increase. The change in the load capacity appears linear. In the micro-spindle, if the axial cutting force which is balanced by the thrust bearing is known, the axial displacement and axial stiffness can be obtained. This information is necessary and will serve as input data for the dynamic design of the micro spindle. As shown in Fig. 6, the axial stiffness varies from 5.1×10^6 N/m to 5.9×10^6 N/m. The average value of 5.5×10^6 N/m will be taken later for the input for the dynamic analysis.

Another issue related to the micro thrust bearing is the bending stiffness generated by the tilting motion of the thrust plate. In this case, the bending stiffness is used as the input data for lateral dynamic characteristics analysis, instead of the axial dynamic analysis. By using the film thickness expression for the titling motion, Eq. (9), the pressure distribution can be obtained. By employing the pressure distribution from this section, the bending stiffness of the micro thrust bearing can be obtained from Eq. (17). The average bending stiffness of the thrust bearing is about 400 N×m/rad, which is relatively small compared to the radial stiffness of the micro journal bearings (e.g., usually more than 1×10^7 N/m).

3.3 Micro journal bearings—numerical simulation and discussion

By employing the proposed method, the dynamic characteristics of the micro journal bearing are studied. The obtained results will, again, be employed as inputs for the spindle rotor dynamic analysis later in the paper. In this section, the originally designed micro bearing reported in Ref. [2] will be analyzed first followed by the analysis of a newly modified design. The obtained data will be transmitted into the dynamic design of the micro-spindle system.

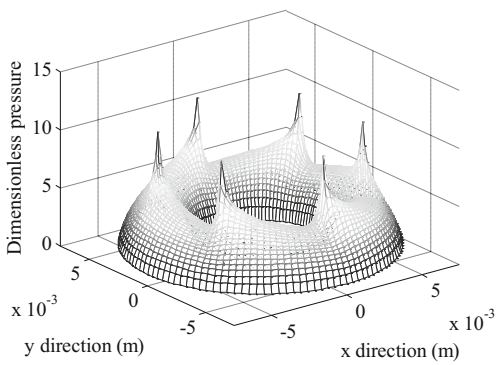

Fig. 5 Pressure distribution of in the micro externally pressurized thrust bearing: the thrust pad is located in the *middle* of the bearing

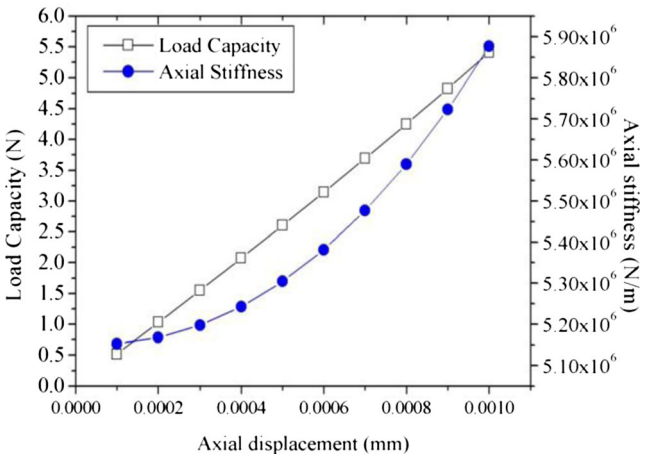

Fig. 6 Variation of the load capacity and axial stiffness of the micro thrust bearings

3.3.1 Case study I: original micro bearing design

The fundamental parameters for the micro journal bearing are presented in Table 2. There are two different micro journal bearings in the original design [2]. The parameters in Table 2 are the common parameters for the two bearings. The detailed diagrams for the two bearings are presented in Fig. 7. The nominal clearance of the journal bearings is 4 μm. The clearance is relatively small as compared to the dimension of the journal radius, so that the change of the clearance due to the centrifugal force should be considered. In Ref. [2], the clearance was decreased to 2.75 μm, which will be used as the nominal clearance in the present analysis of the micro journal bearings.

By solving the dimensionless Reynolds equation Eq. (6) in Section 3.1, the pressure distribution can be obtained. The pressure distributions for no. 1 μ journal bearing for different values of the eccentricity are presented in Fig. 8. As shown in Fig. 8a, when the eccentricity equals to 0, the shaft is located in the center of the bearing. Six peak pressures exist at the locations of the orifices. As the clearance is small, the pressure at the orifices nearly equals the inlet pressure. These high pressure domains around the orifices provide most of the load capacity and stiffness. When an eccentricity exists, the pressure distribution is shown in Fig. 8b, where the aerostatic effect and self-acting effect are coupled. The pressure in the smaller bearing clearance areas are enhanced by the rotation effect.

In Fig. 9, the variation of the load capacity and bearing stiffness with eccentricity is presented. As the eccentricity increases, the load capacity and axial stiffness increase with an approximately linear trend for the load capacity.

For bearing no. 2, the pressure distribution and the load capacity and stiffness are shown in Figs. 10 and 11. The same observations as for bearing no. 1 discussed above apply.

Based on the proposed method, the dynamic characteristics of the micro journal bearings for the original design are analyzed. The analysis of pressure distributions indicates that the hybrid effect cannot be ignored. The obtained load capacity and stiffness for the bearing constitute essential input data for the spindle dynamic analysis.

Table 2 Fundamental parameters for the micro journal bearing

Variable	Value
Diameter of the bearing	7 mm
Length of the bearing	16 mm
Rotating angular speed	600,000 rev/min
Absolute viscosity of air	1.73×10^{-5} N•s/m^2
Radius clearance for the bearing	4 μm
Radius clearance considering the centrifugal force	2.75 μm
Diameter of the journal bearing orifice	0.075 mm
Supply pressure	1.11 MPa

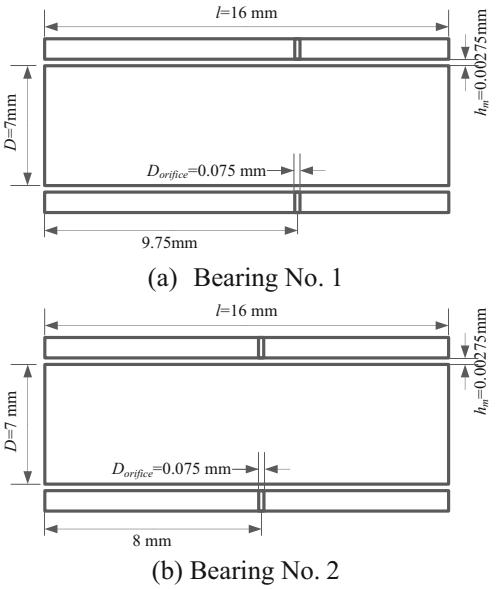

Fig. 7 The structural diagram of the two micro journal bearings in the original design

3.3.2 Case study II: modified micro bearing design

Based on the analysis in Section 3.3.1, the stiffness of the original design micro bearing is about 4.28×10^7 N/m. In the

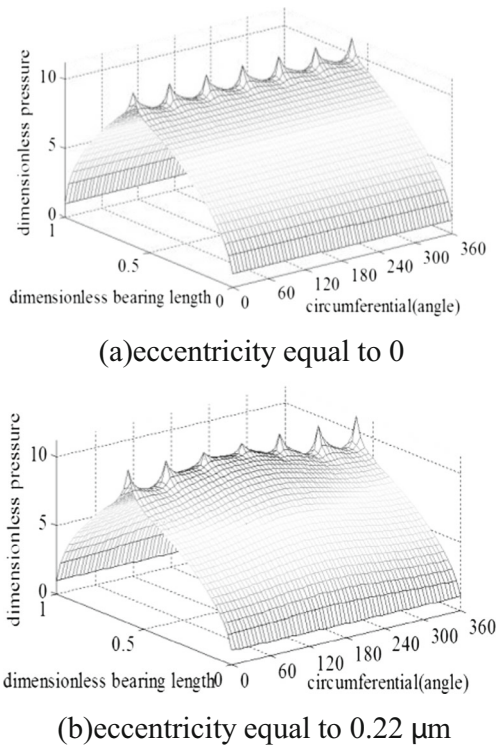

Fig. 8 Pressure distribution for the original design no. 1 journal bearing with the aerostatic and self-acting effect coupled

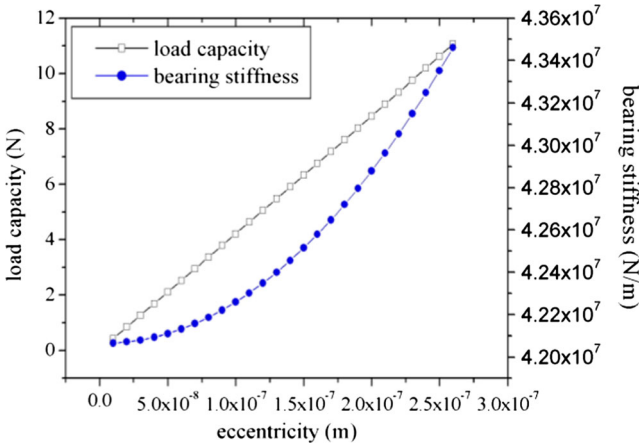

Fig. 9 Variation of load capacity and stiffness with eccentricity for no. 1 journal bearing

rotor dynamic simulation to be introduced later in this paper, this value will be proven insufficient based on the critical speed analysis. More details in support of this assertion will be presented in Section 4. Consequently, the structure of the micro journal bearing needs to be improved with the goal of increasing its stiffness. A plausible solution method for accomplishing this is to increase the number of columns of orifices in the micro journal bearing.

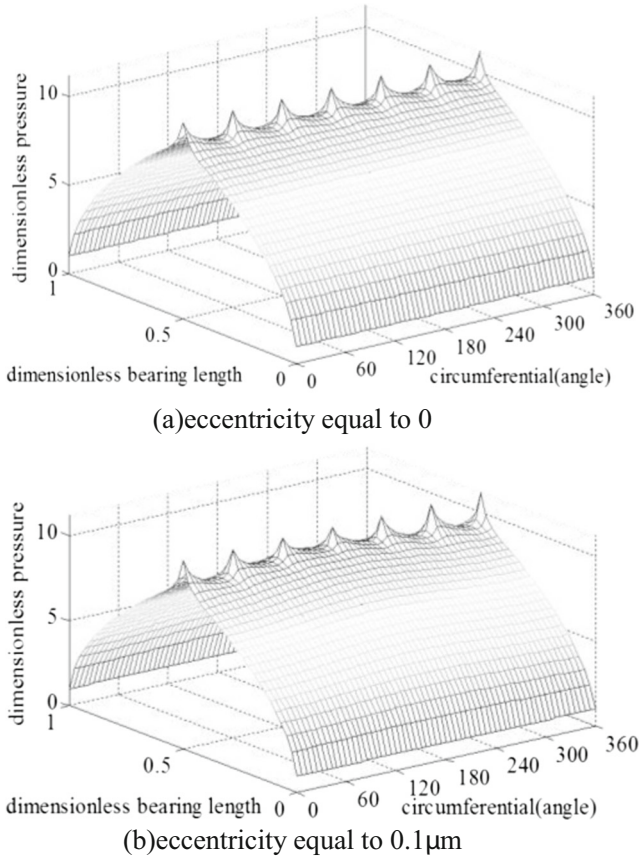

Fig. 10 Pressure distribution for the original design no. 2 journal bearing with aerostatic and self-acting effect coupled

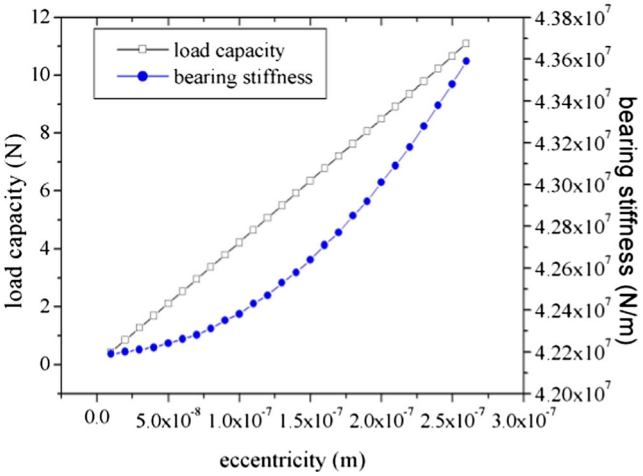

Fig. 11 Variation of load capacity and stiffness with eccentricity for no. 2 journal bearing

The detailed structural diagram of the proposed modified design of the micro journal bearing is presented in Fig. 12. The main difference from the original design is that the structure of bearings no. 1 and no. 2 is assumed identical. In addition, the two columns of orifices are used in the modified design. The distance between the bearing end and the adjacent orifice is 4.0 mm. The other parameters in the modified design are the same as for the original design, as presented in Table 2. The modified design will again be evaluated based on the proposed analysis method in Section 3.1.

The pressure distributions for the modified design for different eccentricities are presented in Fig. 13. In order to compare the effect of the employed changes, the same eccentricities, i.e., of 0 and 0.22 μm, as used for the original design in Fig. 8, were again simulated. As shown in Fig. 13a, 12 peak pressures are located at the positions of the orifices. Compared to the bearings with one column of orifices, a high pressure region is generated between the two orifice columns indicating that the stiffness may be increased. At the eccentricity of 0.22 μm, the high pressure domain still exists in the middle of the bearing. The hybrid effect appears more prominently in the modified design, which increases the pressure at the small clearance locations and decreases the pressure at large clearance locations. Details of about the hybrid effect are presented in Fig. 13b.

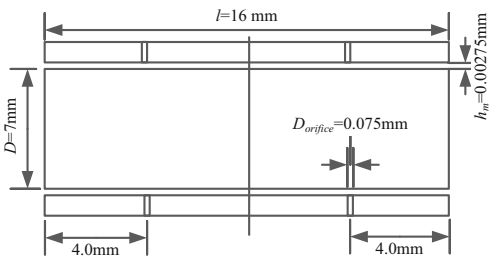

Fig. 12 The structural diagram for the modified micro journal bearing design

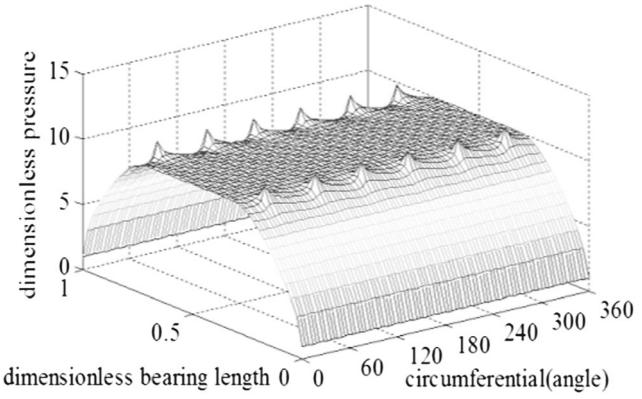

(a)eccentricity equal to 0

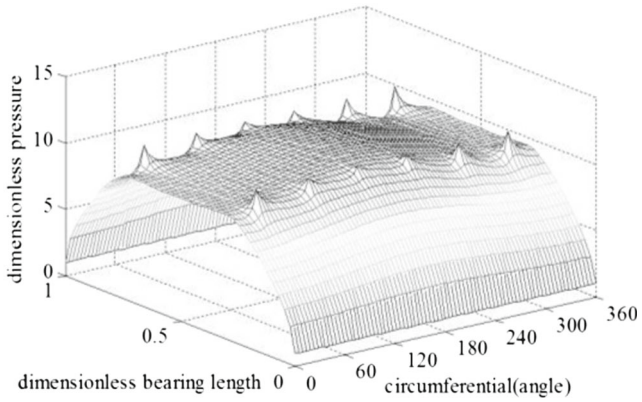

(b)eccentricity equal to 0.22μm

Fig. 13 Pressure distribution for the modified design with aerostatic and self-acting effects coupled

The variation of the load capacity and stiffness with eccentricity for the modified design is presented in Fig. 14. As the eccentricity increases, the load capacity and stiffness increase, again nearly linearly for the load capacity. The trends of the stiffness and load capacity for the modified design are similar to the case of the original design. By increasing the number of columns of orifices, the average stiffness of the journal bearing increased from 4.28×10^7 N/m to 5.24×10^7 N/m. The effects of this incremental increase in stiffness will be discussed in the following section.

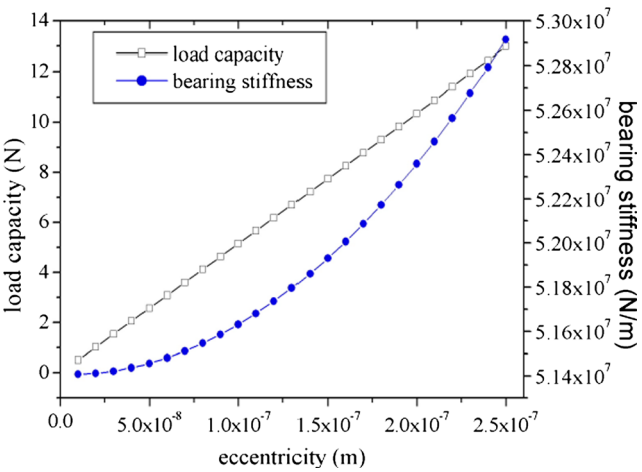

Fig. 14 Variation of load capacity and stiffness with eccentricity for the modified design

By comparing the pressure distribution of the original design (Fig. 8) and of the modified design (Fig. 13), it can be seen that the high pressure region cannot be significantly enlarged. The reason for this is that for the small clearances involved, the pressure generated by the flow between the orifices is relatively high; hence, an increase in the number of columns of orifices from two to more cannot effectively increase the stiffness. Based on the above analysis, two columns of the orifices are enough for the dynamic improvement.

4 Rotor dynamic design and run-out analysis of the micro-spindle system

In Section 3, the dynamic modeling and simulation methodology for the micro air bearings was presented and their dynamic characteristics were obtained by numerical simulation. The results of this analysis will be applied in this section as inputs for the rotor dynamics analysis. The sections below will introduce the design methodology for the dynamics of the micro-spindle system. The main issues that will be addressed include:

(1) The elastic deformation of the rotor given the very high rotating speeds. In conventional studies related to rotor dynamic analysis the rotor is usually assumed as a rigid body;
(2) The gyroscopic effects that cannot be ignored for the same reason as in (1) above;
(3) The spindle's run-out. In mMTs, given the high accuracy requirements, the micro-spindle design imposes rigorous requirements on run-out. The static equilibrium position and whirling amplitudes for the spindle rotor need to be very elaborately considered and designed.

4.1 Modeling method for the rotor system of the micro-spindle

4.1.1 Modeling of the lateral vibrations

The modeling method for rotor dynamic analysis has been addressed by many researchers, and nowadays the finite element method is the most popular means to model the rotor system. Genta [26] introduced the modeling method for the equations of motion based on the complex coordinate method, which has the advantage of high accuracy and efficiency. The discretization means for the equations of motion is the finite

element method. The modeling method in this paper is based on the above method.

The generalized equation of motion for the rotor system based on complex coordinates is [26]:

$$\boldsymbol{M}\ddot{\boldsymbol{q}} + (\boldsymbol{C}_n + \boldsymbol{C}_r - i\Omega\boldsymbol{G})\dot{\boldsymbol{q}} + \left(\boldsymbol{K} + \boldsymbol{K}_\Omega\boldsymbol{\Omega}^2 - i\Omega\boldsymbol{C}_r\right)q = \Omega^2\boldsymbol{f}_r e^{i\Omega t} + \boldsymbol{f}_n(t) \tag{18}$$

where $\boldsymbol{M}$ is the mass matrix of the rotor system, $\boldsymbol{C_r}$ is the rotating damping matrix (such as material damping), $\boldsymbol{C_n}$ is the non-rotating damping matrix (such as bearing damping), $\boldsymbol{G}$ is the gyroscopic matrix, $\boldsymbol{K}$ is the stiffness matrix of the rotor system, $\boldsymbol{q}$ is the generalized complex coordinate, $\boldsymbol{K_\Omega\Omega^2}$ is the additional stiffness caused by the centrifugal force, and $\boldsymbol{f_r}$ and $\boldsymbol{f_n}(t)$ are the force vectors of the unbalanced mass force and other transient non rotating generalized forces.

By separating the real and imaginary parts of Eq. (18), the dynamic equation of motion of the spindle rotor system in real coordinates is given by [26]:

$$\begin{bmatrix}\boldsymbol{M} & 0\\ 0 & \boldsymbol{M}\end{bmatrix}\boldsymbol{X} + \left(\Omega\begin{bmatrix}0 & \boldsymbol{G}\\ -\boldsymbol{G} & 0\end{bmatrix} + \begin{bmatrix}\boldsymbol{C} & 0\\ 0 & \boldsymbol{C}\end{bmatrix}\right)\boldsymbol{X} + \left(\begin{bmatrix}\boldsymbol{K} + \boldsymbol{K}_\Omega\Omega^2 & 0\\ 0 & \boldsymbol{K} + \boldsymbol{K}_\Omega\Omega^2\end{bmatrix} + \Omega\begin{bmatrix}0 & \boldsymbol{C}_r\\ -\boldsymbol{C}_r & 0\end{bmatrix}\right)\boldsymbol{X} = \Omega^2\left[\boldsymbol{f}_{rc}\cos(\Omega t) + \boldsymbol{f}_{rs}\sin(\Omega t)\right] + \boldsymbol{f}_n(t) \tag{19}$$

where $\boldsymbol{X}=[\mathrm{Re}(\boldsymbol{q})^T, \mathrm{Im}(\boldsymbol{q})^T]^T$ is an unknown vector, $\boldsymbol{C}=\boldsymbol{C_r}+\boldsymbol{C_n}$ is the total damping, $\boldsymbol{f_{rc}}=[\mathrm{Re}(\boldsymbol{f_r})^T, \mathrm{Im}(\boldsymbol{f_r})^T]^T$, and $\boldsymbol{f_{rs}}=[-\mathrm{Im}(\boldsymbol{f_r})^T, \mathrm{Re}(\boldsymbol{f_r})^T]^T$ are the sine and cosine part of the unbalanced mass force, $\boldsymbol{f_n}(t)$ is the generalized non rotating exciting force (such as the cutting force during operation of the spindle).

By comparing Eq. (18) and Eq. (19), the equation of motion for the rotor system in complex coordinates is simple. The total number of degrees-of-freedom of the complex dynamic equation is half of the number for the real dynamic equation. Also, the matrix in complex coordinates is symmetrical, which is of significant benefit in numerical simulations. Another advantage of the complex coordinate method is that the solution of Eq. (18) has obvious physical meaning: $\boldsymbol{q}=\boldsymbol{q}_0e^{ist}$ is the rotating vector in the complex plane. Its rotating direction if coincident with the rotor's rotating direction indicates forward whirling while the opposite direction indicates backward whirling.

In modeling of the rotor dynamics for micro-spindles, the beam element is usually chosen as a suitable element. There are different kinds of beam elements including the Euler–Bernoulli and the Timoshenko beam elements. Since shear deformation is included in the Timoshenko beam element, it will be employed in this paper. There are two nodes for the Timoshenko beam element, where each node includes six degrees-of-freedom. The details of the Timoshenko element are presented in Ref. [26], including the stiffness, mass and gyroscopic matrix.

4.1.2 Modeling of axial vibrations

Axial vibrations of the rotor are usually uncoupled from the lateral vibrations implying that they can be studied separately. The axial natural frequency is generally higher than several of the lateral vibration modes and is usually ignored in traditional rotating machinery analysis. But for micro-spindles, given the presence of high frequency exciting/cutting forces along the axial direction, it is necessary to verify the effects of the axial vibrations of the micro-spindle. The equation of motion of the axial vibrations of the spindle rotor can be presented as:

$$\boldsymbol{M}_z\ddot{\boldsymbol{q}}_z + \boldsymbol{C}_z\dot{\boldsymbol{q}}_z + \boldsymbol{K}_z\boldsymbol{q}_z = \boldsymbol{f}_z(t) \tag{20}$$

where $\boldsymbol{M_z}$ is the mass matrix for axial vibrations, $\boldsymbol{C_z}$ is the damping matrix, $\boldsymbol{K_z}$ is the stiffness matrix, $\boldsymbol{q_z}$ is the generalized axial displacement vector, and $\boldsymbol{f_z}(t)$ is the generalized force vector along the axial direction. For axial vibrations of the rotor element, each node has only one single degree of freedom. The only constraint for the system is the axial stiffness from the thrust bearing.

4.2 Simulation methodology for performance analysis

In Section 4.1, the modeling method for the micro-spindle rotor system has been presented. The simulation methodology for the dynamic analysis needs to be carried out next. The motion of the spindle is composed of two parts: (a) the static equilibrium position of the rotor bearing system that depends on the forces acting on the spindle (such as gravity and cutting forces) and the structure of the rotor system, and (b) the whirling motion around the static equilibrium position influenced by the unbalanced response of the spindle. In order to minimize the run-out of the micro-spindle caused by the above factors, the deformation of the tool clamping end of the spindle needs to be decreased to lead to more accurate centering for the cutting operation. This implies that moving the critical speeds away from the operating speed can minimize the unbalanced mass response. The following subsections will introduce methods for realizing these aims.

4.2.1 Deformation analysis

The deformation of the spindle can be calculated from the deformation equation of the micro-spindle. By

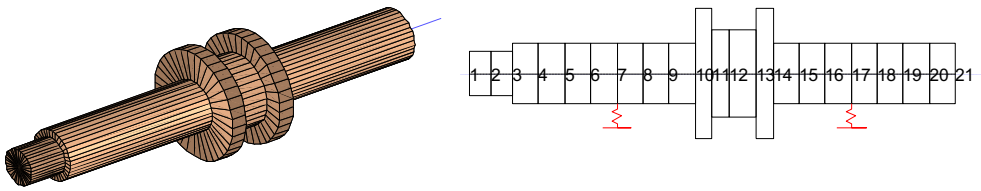

Fig. 15 Model of the rotor for micro-spindle

(a) three dimensional perspective (b) two dimensional perspective

ignoring the rotating force that is caused by the unbalanced mass and the derivative terms of the generalized coordinates in Eq. (18), the deformation equation is presented as follows:

$$\left(\boldsymbol{K}+\boldsymbol{K}_{\Omega}\Omega^2-i\Omega\boldsymbol{C}_r-i\boldsymbol{K}_r^{''}\right)\boldsymbol{q}=\boldsymbol{f}_n(t) \tag{21}$$

where $\boldsymbol{K}_r^{''}$ is the hysteretic damping matrix, which is related to the rotating part of the spindle, and $\boldsymbol{K}_{\boldsymbol{\Omega}}$ is the additional stiffness matrix caused by the centrifugal forces. By solving Eq. (21), the deformation of the spindle rotor can be obtained, which is a spatial curve. The rotor is whirling around the spatial curve with a bow rotatory motion. In this analysis procedure, the support stiffness of the bearing can be assumed as a rigid support implying an infinite stiffness. Then the deformation of the rotor and the reaction force of the support can be calculated. The reaction force is the load of the supporting bearing.

4.2.2 Critical speed and modal shape analysis

The critical speed is a particular phenomenon that exists in rotating machinery, and it is different from the natural frequency. The natural frequency of the rotating spindle is varying with the rotating speed due to the change of the stiffness that is caused by gyroscopic effects. Another important feature in rotating spindles is the special exciting force which is caused by the unbalanced mass and it varies with the rotating speed. Once the natural frequency coincides with the rotating speed, severe resonance occurs with large amplitudes.

The solution of Eq. (18) is composed of the general solution of the homogeneous equation and the particular solution of the inhomogeneous equation, where the damping of the system is ignored. By substituting the form $\boldsymbol{q}=\boldsymbol{q}_0e^{i\Omega t}$, the following equation can be obtained:

$$\left(-\Omega^2(\boldsymbol{M}-\boldsymbol{G}-\boldsymbol{K}_{\Omega})+\boldsymbol{K}\right)\boldsymbol{q}_0=0 \tag{22}$$

The critical speed can be obtained by solving for the eigenvalues of Eq. (23) from:

$$det\left(-\Omega^2(\boldsymbol{M}-\boldsymbol{G}-\boldsymbol{K}_{\Omega})+\boldsymbol{K}\right)=0 \tag{23}$$

The eigenvalues and eigenvectors of the rotor system correspond to the critical speeds and modal shapes of the rotor, respectively. The Campbell diagram presents the natural frequency of the rotor system varying with the rotating speed. So the critical speed can also be obtained from the Campbell diagram. There are numerous sources in the literature that have introduced the Campbell diagram, which will not be discussed in detail in this paper.

4.2.3 Dynamic response and run-out analysis

There are two ways to obtain the dynamic response of the rotor system: one is the frequency domain solution for linear analysis, the other is the time domain solution for nonlinear analysis. For the time domain solution, the Runge–Kutta [26] and Newmark [23] method are widely employed for the solution of Eq. (20). In this section, the frequency domain method is presented. Similar to the critical speed analysis, the solution form of $\boldsymbol{q}=\boldsymbol{q}_0e^{i\Omega t}$ is substituted into Eq. (20) to obtain:

$$\left(-\Omega^2(\boldsymbol{M}-\boldsymbol{G}-\boldsymbol{K}_{\Omega})+i\Omega\boldsymbol{C}_n+\boldsymbol{K}\right)\boldsymbol{q}_0=\Omega^2\boldsymbol{f}_r \tag{24}$$

from which the dynamic response caused by the unbalanced mass can be obtained as follows:

$$\boldsymbol{q}_0=\left(-\Omega^2(\boldsymbol{M}-\boldsymbol{G}-\boldsymbol{K}_{\Omega})+i\Omega\boldsymbol{C}_n+\boldsymbol{K}\right)^{-1}\Omega^2\boldsymbol{f}_r \tag{25}$$

For the micro spindle, the run-out equals to the dynamic response of the system.

Table 3 Load of the micro journal bearing

	Load (*N*)	
	Micro bearing no.1	Micro bearing no.2
Without cutting force	− 0.1180	−0.0795
With cutting force	−9.4657	4.2683

Table 4 The value of axial natural frequency for micro-spindle

The order	The value of axial natural frequency (Hz)
1	2,481.1
2	51,107.8
3	77,124.5
4	144,884.6

4.3 Numerical results and discussion

The model of the rotor system for the micro-spindle is established by the methodology outlined above. In this section Timoshenko beam elements are employed for evaluating the rotor presented in Fig. 15. As shown in Fig. 15b, 21 nodes located on the rotor and 20 elements are used. The two micro journal gas bearings located at nodes 7 and node17 are represented in Fig. 15b by spring symbols.

In order to obtain the stiffness of the micro bearing, the load on the bearing needs to be determined first. The load on the bearing is obtained from the deformation analysis, where the rotor system is assumed rigidly supported. The load on the rotor system is from gravity and cutting forces. The maximal cutting force exerted on the rotor is assumed to be 5 N. The load on the two journal bearings for the cases with and without a cutting force is presented in Table 3. The load of the bearing will be used as the input to determine the stiffness of the journal bearing. Based on the performance analysis of the micro journal gas bearing in Section 3.3, the stiffness of the journal bearing is determined: For the original design, the average stiffness for bearing no. 1 is about 4.33×10^7 N/m and the average stiffness for bearing no. 2 is 4.28×10^7 N/m; for the modified design, the average stiffness for the two journal bearings is 5.22×10^7 N/m.

4.3.1 Axial dynamics analysis

In general, the axial dynamics of the micro-spindle is influenced by both the micro thrust air bearing's axial dynamic characteristics, i.e., axial stiffness and the flexural dynamic performance, i.e., the bending stiffness. Since the bending stiffness of the thrust bearing is small (400 N×m/rad; from Section 3.2), the effect of bending stiffness of the thrust bearing on the flexural dynamic property can be ignored. By employing the stiffness data from Section 3.2, the axial natural frequency of the micro-spindle is presented in Table 4. The lowest axial frequency of the micro-spindle is 2,481.1 Hz. In the actual operation of the micro-spindle, if the cutting force contains components along the axial direction with a frequency around the first axial frequency, severe resonance may occur. In this case, the micro thrust air bearing needs to be redesigned to increase its axial dynamic performance.

The modal shapes of the axial vibrations of the spindle are presented in Fig. 16. The modal shapes can aid in the design of the spindle to reduce the run-out at the tool clamping end.

As shown in Fig. 16a, the modal shape for the first axial natural frequency of 2,481.1 Hz is similar to that of a lumped mass stiffness system, where the axial stiffness acts in the middle of the rotor as a spring. The first natural frequency is the only frequency that lies in the plausible working region of the micro-spindle. For example, when using a two-flute end milling tool at about 75,000 rpm and exciting force with a frequency of 2,500 Hz would be created. This in turn could result in unwanted resonance vibrations. However, it would be a simple matter to select a cutting speed

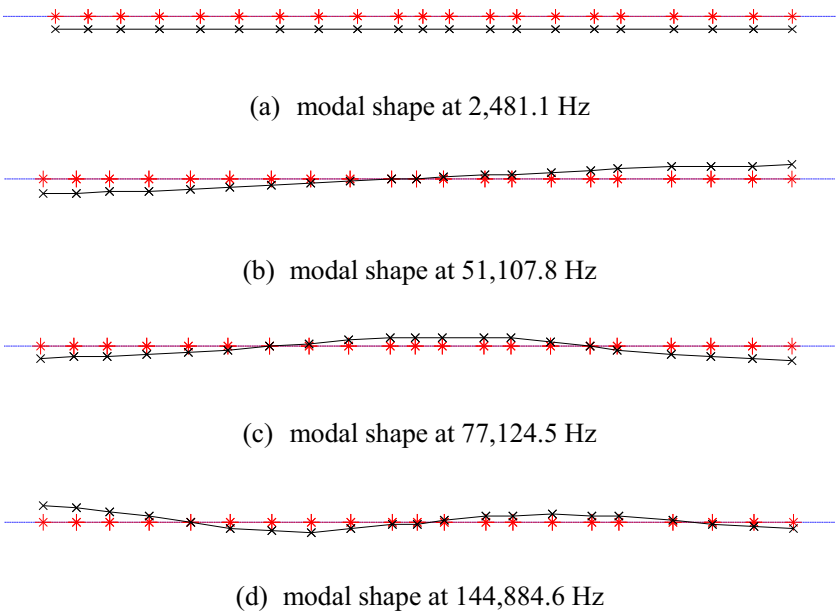

(a) modal shape at 2,481.1 Hz

(b) modal shape at 51,107.8 Hz

(c) modal shape at 77,124.5 Hz

(d) modal shape at 144,884.6 Hz

Fig. 16 Modal shape of the axial vibration for spindle

Table 5 Critical speeds of the micro-spindle with rigidly supported bearings

The order	The value of critical speed (rev/min)
1	643,312.4
2	1,012,168.8
3	1,570,418.7

that would circumvent this problem. The remaining axial natural frequencies are well-beyond technologically feasible cutting conditions.

4.3.2 Flexural dynamics analysis

Based on the modeling method of the rotor dynamics and the parameters of the micro air bearing, the flexural vibration characteristics of the micro-spindle rotor system can be obtained. Firstly, the support of the rotor system is assumed as rigid. This assumption presents the limiting case for the micro-spindle. The critical speeds of the spindle system under the rigid support bearing assumption are presented in Table 5. The first critical speed is about 643,312.4 rev/min, which is close to the operating speed of 400,000 rev/min. For the rigidly supported bearing assumption, the stiffness of the bearing is infinite, which indicates that the maximal critical speed is this value. For the design procedure, if the operating speed is selected above 650,000 rev/min, no improvement in the design of the micro bearing will work. The bearing would have to be redesigned in terms of the structural parameters of the rotor to accommodate the operating speed range.

Case study I: original design By taking the stiffness of the micro air journal bearing into the system of the micro-spindle, the dynamic performance of the originally designed micro-spindle system can be obtained. The critical speeds of the rotor with elastic supports are presented in Table 6, where the eigenvalue analysis is carried out. The critical speeds decrease when the stiffness of the micro journal bearing is included. The first critical speed of the spindle is about 406,497.1 rev/min, which is coincident with the maximal rotating speed obtained in the experiments (414,000 rev/min). In the experimental study, when the spindle speed was increased to approximately 420,000 rev/min, the run-out of the spindle become unacceptable and the rotating speed could not be further

Table 6 Critical speeds of the originally designed micro-spindle

The order	The value of critical speed (rev/min)
1	406,497.1
2	576,194.3
3	731,451.0

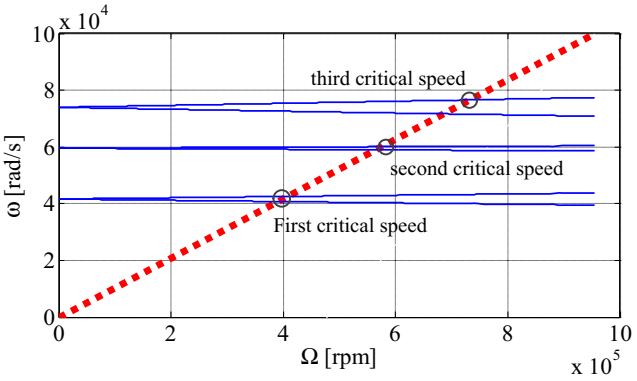

Fig. 17 Campbell diagram for the rotor of micro-spindle

increased. Since the operating speed did not cross the first critical speed, the estimated critical speed cannot be proven by the experimental data. But, the comparison of the simulated and experimental results indicates that the micro-spindle is operated around its first critical speed. Based on this conclusion, it is evident that improvements are needed to reduce the run-out of the micro-spindle.

The Campbell diagram for the elastic supported micro-spindle rotor system is presented in Fig. 17, where the stiffness of the micro journal bearing is included. The critical speed obtained from the Campbell diagram is the same as from the results of the eigenvalue analysis. As shown in Fig. 17, the solid line presents the flexural natural frequency varying with the rotating angular speed. The dotted line signifies that the natural frequency is equal with the rotating speed. The points of intersection between the two lines present several orders of critical speeds. For the critical speeds presented in Fig. 17, a particular order of the critical speed has two intersection points. The bigger critical speed corresponds to the forward whirling critical speed, while the smaller one corresponds to the backward whirling critical speed. In actual cases, the backward whirling critical speed is ignored, which is suppressed by the damping of the system. So in this paper only the forward whirling critical speed is retained for analysis.

The modal shapes of the micro-spindle rotor are presented in Fig. 18. As shown in Fig. 18a, the maximal displacement of

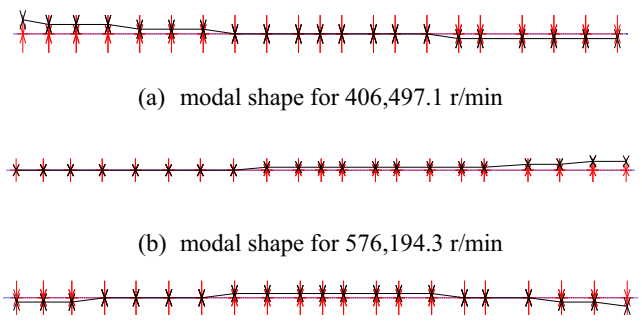

(a) modal shape for 406,497.1 r/min

(b) modal shape for 576,194.3 r/min

(c) modal shape for 731,451.0 r/min

Fig. 18 Modal shape of the flexural vibration for spindle

Table 7 Comparison of the static equilibrium position at tool clamping end of the micro-spindle

	Static equilibrium position of clamped end (m)		Improvement percentage
	Original design	Modified design	
Without cutting force	7.187×10^{-9}	6.545×10^{-9}	8.923 %
With cutting force	1.640×10^{-6}	1.556×10^{-6}	5.141 %

the rotor occurs at the tool clamping end, which will determine the run-out of the spindle. So the first critical speed is the most significant dynamic property for the design of the micro-spindle. For the other critical speeds, e.g., the second and third, that are shown in Fig. 18b, c, the modal displacements are relatively small and the operating speed is far away from these critical speeds; hence, they need not be considered. In further developments of the micro-spindle, if the operation speed is above the first or second critical speed, the modal shape should be studied carefully and designed properly.

In order to reduce the run-out of the micro-spindle, the dynamic response and static equilibrium position of the rotor system should be determined and analyzed. These two issues will be presented in the next section, where a comparison will also be presented.

Case study II: modified design The static equilibrium position of the tool clamping end of the micro-spindle rotor determines the operating position of the spindle shaft. In the design procedure, the static equilibrium position should be as small as possible. The comparison of the static equilibrium positions for the original and the modified designs is presented in Table 7. As shown in Table 7, when the cutting force is not considered, the static equilibrium position is small, i.e., about 10^{-9} m. For the modified design, the static equilibrium position becomes smaller, and the improvement percentage reaches about 8.9 %. If the cutting force is included, the static equilibrium position obviously increases. The modified design results in an improvement of 5.1 %. From the above analysis, it can be concluded that redesigned bearings can improve the static equilibrium position, which will reduce the run-out of the spindle for the operation position.

The comparison of the critical speeds between the original and modified designs is presented in Table 8. It indicates that the critical speed increases as the supported bearing stiffness increases. The first critical speed of the modified design is still around the 400,000 rev/min, but the difference between the two critical speeds is obvious. From experience in designing

Table 8 Comparison of critical speeds between the original and modified designs

Unit (rev/min)	Original design	Modified design
First critical speed	406,497.1	431,711.8
Second critical speed	576,194.3	627,952.3
Third critical speed	731,451.0	748,369.7

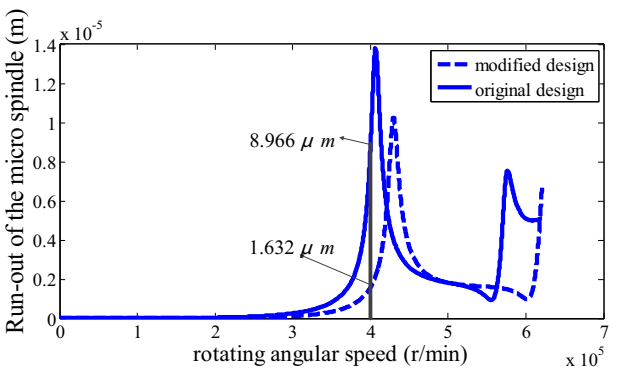

(a) Tool clamping end

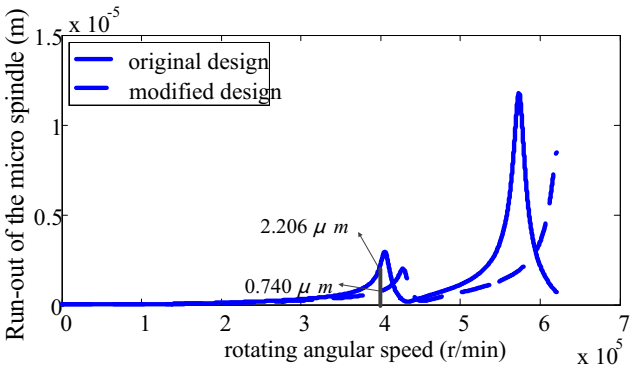

(b) Bearing No. 1

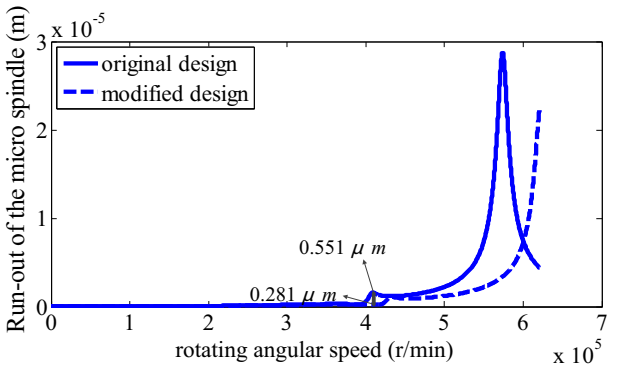

(c) Bearing No. 2

Fig. 19 Comparison of the run-out of the original and modified designs at different locations

Table 9 Comparison of the run-out between the original and modified designs

Position	Run-out of the micro-spindle (*s*)		Reduction percentage (%)
	Original design	Modified design	
Clamping end	8.966	1.632	82.0
Bearing no.1	2.206	0.740	66.5
Bearing no.2	0.551	0.281	49.0

rotating machinery, if the operating speed is near the critical speed, any small change that will keep away from the critical speed can lead to obvious decreases in the dynamic amplitude. More evidence about the validation of the modified design will be acquired in the dynamic response analysis below.

4.3.3 Run-out analysis for the micro spindle

The dynamic response analysis of the micro-spindle will be carried out below and a comparison will be presented. To carry out the analysis, the unbalanced mass and eccentricity need to be defined. Unbalance mass and eccentricity exists in any rotating machinery and cannot be eliminated. These parameters are also hard to obtain from experiments. Fortunately, the rotating shaft has the requirement of balancing quality, which can be used as the input for the unbalanced mass and eccentricity. The total weight of the rotor of the micro-spindle is 0.0161 kg. The eccentricity of the residual mass is 1×10^{-7} mm. Then, the unbalanced parameter for the micro-spindle is 1.61×10^{-9} kg×m.

The dynamic response of the micro spindle corresponds to the run-out of the system without any cutting force acting on the spindle. The comparison of the run-out between the original and modified designs for different locations is presented in Fig. 19, where the tool clamping end, i.e., bearing no. 1, and bearing no. 2 are included. When the rotating speed increases to the critical speed, the peak value of the run-out obviously increases, and this will result in incremental increases in the run-out. As shown in Fig. 19a, even small enhancements in the critical speed lead to very significant decreases in the run-out of the spindle. Since the operating speed is far away from the critical speed in the modified system design, a marked reduction in run-out is observable. A similar situation can be observed in Fig. 19b, c, as well. The details of the run-out reduction effect are presented in Table 9. The tool clamping end is the most relevant position as far as the run-out of the spindle is concerned. The result indicates that the run-out of the micro spindle was reduced from 8.966 to 1.632 μm by the modified design resulting in an 82 % improvement.

5 Summary of the dynamic design methodology

Based on the theoretical and numerical analyses introduced above, the dynamic design methodology for high speed micro-spindles is summarized and presented in Fig. 20. The design methodology is divided into two parts: (a) the design methodology for the micro air bearings and (b) for the rotor system. The connection between the two parts is the bearing load, bearing stiffness, and rotating speed. An iterative procedure is employed to update the parameters of the micro bearing and rotor system until the run-out satisfies the demand. For the design methodology of the micro air bearing, the pressure distributions of the journal and thrust bearings are

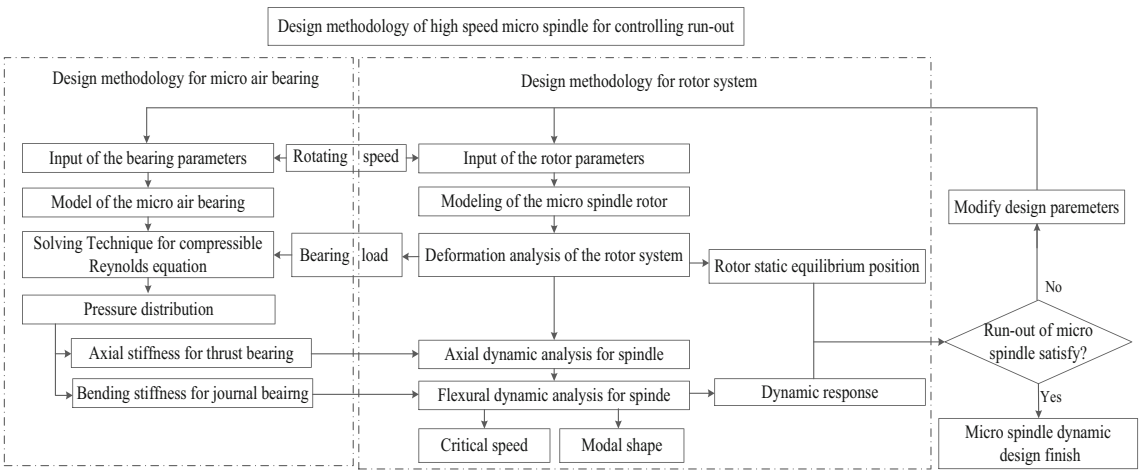

Fig. 20 Flow chart of the dynamic design methodology for high speed micro-spindle

Table 10 Typical computation time for dynamic design

Dynamic design type	Computational time (s)
Deformation analysis	0.003
Axial dynamic analysis	0.108
Critical speed analysis	0.007
Campbell diagram analysis	1.67
Run-out analysis (dynamic response)	5.7

obtained first. The bearing loads obtained from the deformation analysis of the micro-spindle system are used as inputs to obtain the axial and bending stiffness. For the design methodology of the micro-spindle rotor, by taking the stiffness of the bearings into the system, the axial natural frequency of the spindle is obtained. The flexural dynamic analysis of the spindle is carried out to obtain the critical speed, modal shapes and dynamic responses. The rotor static equilibrium position of the spindle is solved by deformation analysis. The static equilibrium position and dynamic response define the run-out of the spindle. The above proposed procedure for the dynamic design methodology makes the foundation for controlling the run-out for high speed micro-spindles.

As introduced in Section 4, the typical computation time is presented in Table 10.

6 Conclusions

A dynamic design methodology for micro-spindles for mMT systems is presented in this paper to obtain ultra-small run-out. Design methodologies for the micro air bearings and the micro-spindle rotor system are included. By employing the Newton iteration method, a modeling and simulation method for externally pressurized micro journal and thrust bearings is formulated, and used to evaluate the pressure distribution and stiffness. The pressure distribution helps in understanding the generation mechanism of the bearing's load capacity and stiffness. The knowledge of the stiffness is an essential input for dynamic analysis of the micro-spindle's rotor dynamics. By employing the finite element method, the model of the micro-spindle rotor is discretized. The dynamic characteristics such as static equilibrium position, critical speeds, and unbalanced responses were acquired to evaluate the run-out of the micro-spindle. By applying the above-mentioned methodologies, a systematic comparative analysis of two micro-spindle designs (termed original and modified) was carried out aimed at reducing spindle run-out. The detailed conclusions are the following:

(1) By increasing the number of columns of orifices in the journal bearing from one to two, the stiffness of the journal bearing increased by 22.4 %; however, a further increase in the number of columns would not significantly increase the stiffness.
(2) The bending stiffness generated by the tilting motion of the thrust plate is relatively small and can be ignored in the dynamic analysis.
(3) By numerical simulation, the first critical speed of the original design is about 406,497 rev/min that is around the maximal rotating speed reached in the experiments. This fact is utilized as the principle to reduce the run-out.
(4) By redesigning the micro journal bearing, the first critical speed was increased by 6.2 %, and the run-out of the micro-spindle was reduced by 82 %, which proves the validity of the proposed dynamic design methodology for controlling the run-out.
(5) The flow chart of the dynamic design methodology for high speed spindles is summarized and it provides a foundation for future designs.

In order to decrease the run-out of the micro-spindle for mMTs, more work needs to be done with focus on the following issues: (a) The experimental verification of the modified design should be carried out. (b) For higher rotating speeds above the critical speed, the addition of damping into the spindle system should be considered to facilitate safely passing the critical speed. (c) The methodologies presented in this paper can be termed as a "passive design method." It will lead to a robust design. However, in future studies, "active control methods" should be explored. For example, the supply pressure could be used as the control parameter. (d) In more sophisticated designs to control the run-out, the cutting force should be included and a nonlinear design procedure should be formulated.

Acknowledgments The research presented here was supported by the National Natural Science Foundation of China (Grant No. 51106035). The authors are grateful for the support.

References

1. Ehmann KF, DeVor RE, Kapoor SG, Cao J (2008) Design and analysis of micro/meso-scale machine tools. In: Smart devices and machines for advanced manufacturing (pp. 283–318). Springer, London
2. Sung H (2007) High-speed fluid bearing micro-spindles for meso-scale machine tools (Doctoral dissertation, Ph. D. Dissertation of the Northwestern University, USA)
3. Anonymous (2008a) http://www.fanuc.co.jp
4. Anonymous (2008b) http://www.atometric.com
5. Brown A (2008) Big stage for a small idea. Mechanical Engineering, April 27–31
6. Zhang SJ, To S (2013) The effects of spindle vibration on surface generation in ultra-precision raster milling. Int J Mach Tools Manuf 71:52–56
7. Martin DL, Tabenkin AN, Parsons FG (1995) Precision spindle and bearing error analysis. Int J Mach Tools Manuf 35(2):187–193

8. Marsh E, Arneson D, Van Doren MJ, Blystone SA (2005) The effects of spindle dynamics on precision flycutting. In Proceedings of the American society for precision engineering 2005 annual meeting
9. Zhang SJ, To S, Cheung CF, Wang HT (2012) Dynamic characteristics of an aerostatic bearing spindle and its influence on surface topography in ultra-precision diamond turning. Int J Mach Tools Manuf 62:1–12
10. An CH, Zhang Y, Xu Q, Zhang FH, Zhang JF, Zhang LJ, Wang JH (2010) Modeling of dynamic characteristic of the aerostatic bearing spindle in an ultra-precision fly cutting machine. Int J Mach Tools Manuf 50(4):374–385
11. Bhat N, Kumar S, Tan W, Narasimhan R, Low TC (2012) Performance of inherently compensated flat pad aerostatic bearings subject to dynamic perturbation forces. Precis Eng 36(3):399–407
12. Hassini MA, Arghir M (2012) A simplified nonlinear transient analysis method for gas bearings. Trans ASME-F-J Tribol 134(1):011704
13. Otsu Y, Somaya K, Yoshimoto S (2011) High-speed stability of a rigid rotor supported by aerostatic journal bearings with compound restrictors. Tribol Int 44(1):9–17
14. Liu ZS, Zhang GH, Xu HJ (2009) Performance analysis of rotating externally pressurized air bearings. Proc IME B J Eng Manufact 223(4):653–663
15. Zhang GH, Liu ZS, Wang GL, Yan JJ (2011) Analytical forces parameters identification of hybrid journal gas bearing based on transfer function. ASME TurboEXpo 2011:GT2011–GT45788
16. Chen CH, Tsai TH, Yang DW et al (2010) The comparison in stability of rotor-aerostatic bearing system compensated by orifices and inherences [J]. Tribology International 43(8):1360–1373
17. Delhaes GM, van Beek A, van Ostayen RA, Munnig Schmidt RH (2009) The viscous driven aerostatic supported high-speed spindle. Tribol Int 42(11):1550–1557
18. Wang CC (2011) Bifurcation analysis of high speed spindle air bearings. J Vib Control 17(1):103–114
19. Wang CC, Yau HT (2010) Theoretical analysis of high speed spindle air bearings by a hybrid numerical method. Appl Math Comput 217(5):2084–2096
20. Al-Bender F (2009) On the modeling of the dynamic characteristics of aerostatic bearing films: from stability analysis to active compensation. Precis Eng 33(2):117–126
21. Yang DW, Chen CH, Kang Y, Hwang RM, Shyr SS (2009) Influence of orifices on stability of rotor-aerostatic bearing system. Tribol Int 42(8):1206–1219
22. Zhang GH, Sun Y, Liu ZS, Zhang M, Yan JJ (2012) Dynamic characteristics of self-acting gas bearing–flexible rotor coupling system based on the forecasting orbit method. Nonlinear Dynamics 69(1–2):341–355
23. Guang-hui Z, Yi S, Zhan-sheng L, Fang-cheng X, Jia-jia Y (2011) Application of a forecasting coupling method to the non-linear dynamic analysis of a flexible rotor supported by externally pressurized orifices hybrid gas bearings. Proc Inst Mech Eng Part J: J Eng Tribol 225(8):704–717
24. Schiffmann J, Favrat D (2010) Integrated design and optimization of gas bearing supported rotors. J Mech Des 132:051007
25. Stoud KJ (1996) The design of aerostatic bearings, 1996. Whitestone BusinessCommunications, Nuneaton
26. Genta G (2005) Dynamics of rotating systems. Springer, NY